

MODELING WEAKLY NONLINEAR ACOUSTIC WAVE PROPAGATION

by IVAN CHRISTOV [†]

(*Department of Mathematics, Texas A&M University, College Station,
TX 77843-3368, USA*)

C. I. CHRISTOV

(*Department of Mathematics, University of Louisiana at Lafayette, Lafayette,
LA 70504-1010, USA*)

and P. M. JORDAN [‡]

(*Code 7181, Naval Research Laboratory, Stennis Space Center,
MS 39529-5004, USA*)

[Received 16 May 2007. Revise 20 June 2007. Accepted 23 June 2007]

Summary

Three weakly nonlinear models of lossless, compressible fluid flow—a straightforward weakly nonlinear equation (WNE), the inviscid Kuznetsov equation (IKE) and the Lighthill–Westervelt equation (LWE)—are derived from first principles and their relationship to each other is established. Through a numerical study of the blow-up of acceleration waves, the weakly nonlinear equations are compared to the ‘exact’ Euler equations, and the ranges of applicability of the approximate models are assessed. By reformulating these equations as hyperbolic systems of conservation laws, we are able to employ a Godunov-type finite-difference scheme to obtain numerical solutions of the approximate models for times beyond the instant of blow-up (that is, shock formation), for both density and velocity boundary conditions. Our study reveals that the straightforward WNE gives the best results, followed by the IKE, with the LWE’s performance being the poorest overall.

1. Introduction

The theory of lossless (that is, inviscid, non-heat-conducting) compressible fluids is of considerable interest because of its numerous physical applications. Many models, with varying degrees of complexity and approximation/exactness, can be found in the literature. However, they all are the result of the application of certain simplifications and assumptions (that stem from the physical situation under consideration) to the exact equations of motion for lossless compressible fluids, that is, the Euler equations (1, 2).

In the theory of nonlinear acoustics (3 to 7), the most popular weakly nonlinear approximations are the inviscid Kuznetsov equation (IKE) (8) and the Lighthill–Westervelt equation (LWE)

[†]Present address: Department of Engineering Sciences and Applied Mathematics, Northwestern University, Evanston, IL 60208-3125, USA.

[‡]Corresponding author (pjordan@nrlssc.navy.mil)

(9). These weakly nonlinear (or ‘finite-amplitude’) models have been indispensable in shaping our understanding of the various physical mechanisms at work in such wave phenomena. However, the full extent of the nonlinear effects they embody can only be found through numerical simulation/experimentation.

In (10, 11), we performed a series of numerical simulations of nonlinear acoustic propagation in a one-dimensional (1D) setting. In (10), we showed how the LWE can be solved numerically using the same framework as the Euler equations, that is, that of Godunov-type schemes (12, 13). Subsequently, we showed in (11) that because the LWE is based on the ‘linear-impedance assumption’ (LIA) (4), its ability to correctly describe the cumulative effects of nonlinearity is seriously hindered.

In an effort to better understand the latter results, we present here a first-principles approach to lossless compressible flows under the weakly nonlinear theory—that is to say, we derive an approximate finite-amplitude equation with the least number of assumptions and approximations. In addition, we show how the ‘classical’ approximate models can be obtained from it, and explain the differences. It should be noted here that by a ‘weakly nonlinear model’, we mean an approximate equation in which the nonlinear terms of second order and higher in the Mach number are neglected, under the assumption that the Mach number is sufficiently small.

As in our previous works, we rely on numerical methods to assess the applicability and performance of the approximate models of nonlinear acoustics. It should be noted here that, until recently, numerical studies of these model equations were lacking in the literature (5). Even more scarce were comparative studies, in which the performance of several model equations is evaluated simultaneously—an issue we address in the present work. To the best of our knowledge, the only study of this kind (prior to our work) is that of Kagawa *et al.* (14, 15), who investigated certain problems involving self-focusing apertures using the finite-element method. They attributed the poor performance of LWE to the particular problem being simulated, and thus did not reach the same conclusion that we did in (11), specifically, that the LWE is ‘crippled’ by the LIA. Moreover, the numerical work of Kagawa *et al.* (14, 15) was limited to smooth flows. Thus, the latter authors were unable to fully assess the ability of the IKE and the LWE to capture shock formation and related phenomena, these being the most prominent effects of nonlinearity in hyperbolic equations. This limitation is remedied in the present work by our use of a Godunov-type finite-difference scheme which allows us to numerically solve all the model equations for times beyond the instant of shock formation.

Here, we would like to emphasize the generality and extensibility of our numerical approach. Though simple finite-difference schemes can be used to effectively simulate nonlinear acoustic propagation prior to shock formation (16), such methods break down when large gradients develop in the field variables. To overcome this, we employ a variation of the Monotonic Upstream-centered Scheme for Conservation Laws (MUSCL), which is a shock-capturing Godunov-type scheme, due to Hancock (12), as we did in (10, 11), which is designed to compute discontinuous solutions of generic hyperbolic systems of conservation laws. Thus, after the model equations have been reformulated as conservation laws, we solve all of them with the same numerical method! It should be noted that Inoue and Yano (17) successfully employed a Godunov-type scheme to compare the weakly and fully nonlinear theories in the context of the N -wave problem. However, unlike us, the latter authors employed asymptotic methods to study the weakly nonlinear case. Moreover, it should be noted that, Godunov-type schemes perform as well as the classical finite-difference schemes when the flow is smooth. For example, Godunov-type (finite-volume) schemes have been found to be especially effective for linear acoustics problems in random media (18), where the solutions remain smooth but the governing equations have oscillatory coefficients.

We focus our numerical experiments on the interesting phenomenon of acceleration wave blow-up in finite time. As opposed to a shock wave, which is defined as a propagating surface across which one or more of the acoustic field variables themselves suffer a jump discontinuity, an acceleration wave is defined as a propagating surface across which at least one of the first derivatives of the field variables exhibits a jump discontinuity (19). Our investigation provides support for the conjecture that finite-time blow-up leads to shock formation (20, 21). In this context, Thomas (22) appears to have been the first to determine exact expressions describing the growth (that is, blow-up) and decay of what he called ‘sonic discontinuities’, that is, acceleration waves, in ideal gases using singular surface theory. Subsequently, Elcrat (23), Jordan and Christov (16), Jordan and Straughan (24), as well as the present authors (10, 11), all considered the propagation of acoustic acceleration waves in lossless gases. Additionally, it should be noted that acceleration waves, which are special cases of singular surfaces (19, 25), arise not only in acoustics but also in other areas of continuum mechanics (26 to 34). Furthermore, acceleration wave analysis provides theoretical results that can be used to gauge the reliability and efficacy of numerical schemes (16).

This paper is organized as follows. In section 2, the theory of lossless flow is revisited and a unified derivation of the equations of motion for both perfect gases and a class of barotropic fluids is presented. (Note that a barotropic fluid is one for which the pressure is a function of the density alone (1).) In section 3, we discuss the derivation of the approximation equations of motion under the finite-amplitude assumption. In section 4, we show how the weakly nonlinear equations can be reformulated as hyperbolic systems of conservation laws. Then, in section 5, we provide a number of analytical results, based on the first-order system formulation of the approximate equations, showing why the straightforward weakly nonlinear approximation advocated in this paper is better than the classical ones. In section 6, we compare and contrast the three approximate models and the Euler equations on the basis of numerical simulations of acceleration wave blow-up. Finally, in section 7, we state our conclusions and mention possible future work. In addition, two Appendices are provided for completeness and convenience: In Appendix A we give a brief summary of the Godunov-type scheme used for our calculations; in Appendix B we summarize the standard singular surface analysis of acceleration wave blow-up for the case of a perfect gas.

2. Governing equations

It is generally accepted that the motion of a lossless, compressible fluid is described by the well-known Euler equations (1, 2), which read

$$\rho_t + \nabla \cdot (\rho \mathbf{v}) = 0, \quad (2.1)$$

$$\rho \left[\mathbf{v}_t + \frac{1}{2} \nabla |\mathbf{v}|^2 - \mathbf{v} \wedge (\nabla \wedge \mathbf{v}) \right] + \nabla \wp = 0. \quad (2.2)$$

Here, \mathbf{v} is the velocity vector, $\rho (>0)$ is the mass density, $\wp (>0)$ is the thermodynamic pressure, and all body forces have been omitted. Moreover, since the fluid is lossless, the flow is therefore isentropic, and it follows that $\dot{\eta} = 0$, where η is the specific entropy and a superposed dot denotes the material derivative. However, we now make the additional assumption of homentropic flow, meaning that $\dot{\eta} = 0$ and $\nabla \eta = 0$ (1).

Finally, the equation of state, which is the thermodynamic relation needed to close our system of equations, is of the specific form

$$\wp = \wp(\rho), \quad (2.3)$$

that is, we have a ‘barotropic’ flow (1, 2). Note that the flow of a barotropic fluid is always barotropic, but the converse need not be true. Note also that in the case of a perfect gas undergoing homentropic flow, it can be shown that the equation of state assumes a polytropic form (2), and is thus a particular case of (2.3). However, for fluids in general, especially liquids, it is not always possible to determine the dependence of \wp upon the other field variables (5). Therefore, in such cases, (2.3) would be an assumption.

To further simplify our presentation, let us make the additional assumption that initially, the fluid is in its equilibrium state; that is, at time $t = 0$, we have $\mathbf{v} = \mathbf{0}$, $\varrho = \varrho_0$, $\wp = \wp_0$ and $\eta = \eta_0$, where ϱ_0 , \wp_0 and η_0 are constants. Thus, since the flow is homentropic, assuming initial equilibrium implies not only that $\eta = \eta_0$ for all $t \geq 0$ but also that the flow is always irrotational, that is, $\nabla \wedge \mathbf{v} \equiv \mathbf{0}$ for all $t \geq 0$. Therefore, in the present work, we only consider longitudinal (or acoustic) wave phenomena.

Let us now introduce the following dimensionless variables:

$$\begin{aligned} \{x', y', z'\} &= \{x, y, x\}/L, & t' &= t(c_0/L), & \phi' &= \phi/(u_m L), \\ \wp' &= \wp/(\varrho_0 c_0^2), & \varrho' &= \varrho/\varrho_0, & u' &= u/u_m, \end{aligned} \quad (2.4)$$

where $(0 <) u_m \stackrel{\text{def}}{=} \max |\mathbf{v}|$ and $L (> 0)$ denote a characteristic speed and length, respectively, and c_0 is the sound speed in the undisturbed fluid. In terms of these variables (omitting the primes without fear of confusion), and recalling the irrotational nature of the flow, the governing system of equations becomes

$$\varrho_t + \epsilon \nabla \cdot (\varrho \mathbf{v}) = 0, \quad (2.5)$$

$$\mathbf{v}_t + \frac{1}{2} \epsilon \nabla |\mathbf{v}|^2 + \epsilon^{-1} \varrho^{-1} \nabla \wp = 0, \quad (2.6)$$

$$\wp = \wp(\varrho), \quad (2.7)$$

where $\epsilon \stackrel{\text{def}}{=} u_m/c_0$ is the Mach number.

Since the flow is barotropic, we can introduce the specific enthalpy function

$$h(\varrho) = h_0 + \int_1^\varrho \frac{1}{\hat{\varrho}} \frac{d\wp}{d\hat{\varrho}} d\hat{\varrho}, \quad (2.8)$$

where $\hat{\varrho}$ is a ‘dummy’ integration variable and h_0 is a constant that depends only on the initial state of the fluid (that is, h_0 denotes the specific enthalpy of the fluid in its equilibrium state). Using h , we can now rewrite the pressure gradient term in (2.6) as

$$\frac{1}{\varrho} \nabla \wp = \frac{1}{\varrho} \frac{d\wp}{d\varrho} \nabla \varrho = \frac{dh}{d\varrho} \nabla \varrho = \nabla h. \quad (2.9)$$

Moreover, the conservation of mass equation (2.5) can be recast in the form

$$h_t + \epsilon \mathbf{v} \cdot \nabla h = -\epsilon c^2 \nabla \cdot \mathbf{v}, \quad (2.10)$$

where

$$c^2 = \frac{d\wp}{d\varrho} = \varrho \frac{dh}{d\varrho} \quad (2.11)$$

is the (dimensionless) local speed of sound.

Upon introducing the velocity (or acoustic) potential ϕ , where $\mathbf{v} = \nabla\phi$, into (2.6) and integrating over space, we obtain the following well-known relation between the enthalpy and the potential:

$$h - h_0 = -\epsilon \left(\phi_t + \frac{1}{2}\epsilon |\nabla\phi|^2 \right), \quad (2.12)$$

which is known as the Cauchy–Lagrange integral (2). Similarly, in terms of the potential, (2.10) becomes

$$h_t + \epsilon \nabla\phi \cdot \nabla h = -\epsilon c^2 \nabla^2 \phi. \quad (2.13)$$

Introducing (2.12) into (2.13), we obtain

$$\phi_{tt} + 2\epsilon \nabla\phi \cdot \nabla\phi_t + \epsilon^2 |\nabla\phi|^2 \nabla^2 \phi = c^2 \nabla^2 \phi. \quad (2.14)$$

This is the general expression of the conservation of momentum in terms of the potential function. Note that (2.14) is not closed because c is, at this point, an unknown function of the field variables. But, given the nature of our flow, there are two well-known instances in which c can be expressed (explicitly) in terms of ϕ . The first is the case of a perfect gas and the second is that of a barotropic fluid for which \wp is a quadratic function of ϱ .

2.1 Case of a perfect gas

For the homentropic flow of a perfect gas, (2.3) assumes the following specific (polytropic) form:

$$\wp = \varrho^\gamma / \gamma, \quad (2.15)$$

where the constant $\gamma (>1)$ is the ‘adiabatic index’ (1, 2). Then, from (2.11), we easily obtain $c^2 = \varrho^{\gamma-1}$. Furthermore, we find (by substituting (2.15) into (2.8) and performing the integration) that

$$h = \frac{1}{\gamma-1} \varrho^{\gamma-1} = \frac{1}{\gamma-1} c^2 \implies c^2(h) = (\gamma-1)h, \quad (2.16)$$

which furnishes the needed explicit dependence of c on h , and gives us $h_0 = (\gamma-1)^{-1}$.

Next, using (2.12) to eliminate h from (2.16), we obtain

$$c^2 = 1 - \epsilon(\gamma-1) \left[\phi_t + \frac{1}{2}\epsilon |\nabla\phi|^2 \right]. \quad (2.17)$$

Substitution of the latter into (2.14) yields the following exact, closed-form equation for the potential:

$$\phi_{tt} + 2\epsilon \nabla\phi \cdot \nabla\phi_t = \left[1 - \epsilon(\gamma-1)\phi_t - \frac{1}{2}\epsilon^2(\gamma+1)|\nabla\phi|^2 \right] \nabla^2 \phi, \quad (2.18)$$

which we refer to as the ‘potential Euler equation’ (PEE).

2.2 Case of a barotropic fluid with a quadratic equation of state

Here, the (dimensionless) equation of state is taken to be a quadratic function of the density (5), namely,

$$\wp = \wp_0 + (\varrho - 1) + \frac{1}{2}\alpha(\varrho - 1)^2, \quad (2.19)$$

where α (commonly denoted by B/A) is known as the ‘nonlinearity parameter’ (36) and $\wp_0 = \gamma^{-1}$ is the pressure in the equilibrium state. Equation (2.19) often arises as an approximation to the formal Taylor-series expansion of (2.3).

We begin by substituting (2.19) into (2.8) and performing the integration to find that

$$h - h_0 = (1 - \alpha) \ln \varrho + \alpha(\varrho - 1) \quad (2.20)$$

and $h_0 = \alpha$. Then, after setting $\tilde{\alpha} \stackrel{\text{def}}{=} \alpha/(1 - \alpha)$, we have

$$h(\varrho) = (1 - \alpha)(\ln \varrho + \tilde{\alpha}\varrho) \implies \varrho(h) = \tilde{\alpha}^{-1} W_0[\tilde{\alpha} e^{h/(1-\alpha)}], \quad (2.21)$$

where $W_0(\cdot)$ is the principal branch of the Lambert W -function (35).

Next, we differentiate (2.19) and use (2.21) to find that the square of the sound speed is

$$c^2 = 1 + \alpha(\varrho - 1) = (1 - \alpha)\{1 + W_0[\tilde{\alpha} e^{h/(1-\alpha)}]\}. \quad (2.22)$$

Using (2.12) to eliminate h from the latter, we obtain

$$c^2 = (1 - \alpha) \left\{ 1 + W_0 \left(\tilde{\alpha} \exp \left[\tilde{\alpha} - \frac{\epsilon}{1 - \alpha} \left(\phi_t + \frac{1}{2} \epsilon |\nabla \phi|^2 \right) \right] \right) \right\}, \quad (2.23)$$

which furnishes the explicit relation between c and ϕ , needed to close (2.14). Therefore, the resulting exact, closed-form equation for the potential is

$$\begin{aligned} \phi_{tt} + 2\epsilon \nabla \phi \cdot \nabla \phi_t = \\ (1 - \alpha) \left\{ 1 - \frac{\epsilon^2}{1 - \alpha} |\nabla \phi|^2 + W_0 \left(\tilde{\alpha} \exp \left[\tilde{\alpha} - \frac{\epsilon}{1 - \alpha} \left(\phi_t + \frac{1}{2} \epsilon |\nabla \phi|^2 \right) \right] \right) \right\} \nabla^2 \phi, \end{aligned} \quad (2.24)$$

which appears to be a new result.

Clearly, (2.24) is quite complicated and likely intractable. Fortunately, we can derive a simpler, albeit approximate, equation by assuming that $\epsilon \ll 1$. Under this assumption, an inspection of (2.12) indicates that the relative change in the enthalpy will be of the same order, that is, $h - h_0 = \mathcal{O}(\epsilon)$. Thus, one can use the Taylor-series expansion of the W -function (35) in terms of h about the equilibrium value h_0 to simplify the right-hand side of (2.22):

$$\begin{aligned} \varrho = \tilde{\alpha}^{-1} W_0[\tilde{\alpha} e^{h/(1-\alpha)}] &= \tilde{\alpha}^{-1} W_0[\tilde{\alpha} e^{h_0/(1-\alpha)}] + \frac{\tilde{\alpha}^{-1} W_0[\tilde{\alpha} e^{h_0/(1-\alpha)}]}{(1 - \alpha)\{1 + W_0[\tilde{\alpha} e^{h_0/(1-\alpha)}]\}} (h - h_0) \\ &+ \mathcal{O}[(h - h_0)^2]. \end{aligned} \quad (2.25)$$

Recalling that $h_0 = \alpha$, $\tilde{\alpha} \equiv \alpha/(1 - \alpha)$ and using the identity $W_0(\zeta e^\zeta) = \zeta$ (35), (2.25) simplifies to

$$\varrho = 1 + (h - h_0) + \mathcal{O}(\epsilon^2). \quad (2.26)$$

Then, within the same order of approximation with respect to the Mach number, we obtain

$$c^2 = 1 + \alpha(\varrho - 1) \approx 1 + \alpha(h - h_0) = 1 - \epsilon \alpha \left(\phi_t + \frac{1}{2} \epsilon |\nabla \phi|^2 \right), \quad (2.27)$$

where the last equality follows from (2.12). At this point, it should be clear that upon introducing the latter relation into (2.14), the equation for the potential that we obtain is identical to (2.18) with

$\gamma - 1$ replaced by α . This is not surprising; in the case of a perfect gas, α is related to the adiabatic index by $\alpha = \gamma - 1$ (3, 5, 36). (One can easily show this by expanding (2.15) in a Taylor series and matching the resulting coefficients to those in (2.19).)

Thus, we can use (2.18) for the homentropic flows of both perfect gases (for arbitrary Mach numbers) and barotropic fluids with a quadratic equation of state (for sufficiently small Mach numbers). Again, we emphasize that (2.24) is valid for arbitrary Mach number values, but it is of limited use due to its complicated form. Finally, we note that the assumption $\epsilon \ll 1$, which is the basis of the finite-amplitude approximation, is used in section 3 to derive approximate versions of (2.18).

3. Finite-amplitude approximations in one dimension

For the remainder of this paper, we restrict ourselves to 1D homentropic flow of a perfect gas along the x -axis (that is, we assume $\mathbf{v} \equiv \nabla\phi = (u(x, t), 0, 0)$). Thus, (2.5), (2.6) and (2.15) become

$$\rho_t + \epsilon u \rho_x + \epsilon \rho u_x = 0, \quad (3.1)$$

$$\rho(u_t + \epsilon uu_x) + \epsilon^{-1} \wp_x = 0, \quad (3.2)$$

$$\wp = \rho^\gamma / \gamma. \quad (3.3)$$

Similarly, the PEE, given by (2.18), reduces to

$$[1 - \epsilon(\gamma - 1)\phi_t]\phi_{xx} - 2\epsilon\phi_x\phi_{tx} - \phi_{tt} = \frac{1}{2}\epsilon^2(\gamma + 1)(\phi_x)^2\phi_{xx}. \quad (3.4)$$

This equation appears in a number of works (3 to 5, 10, 11) and has many applications—for example in the study of acoustic waves and nonlinear resonances in organ pipes (37).

At this point, it is common to make use of the finite-amplitude (or weakly nonlinear) assumption, that is, $0 < \epsilon \ll 1$, to derive simpler, but approximate, versions of (3.4). Below, we discuss three model equations that result from this assumption.

3.1 Consistent weakly nonlinear approximation

Upon neglecting terms that are $\mathcal{O}(\epsilon^2)$ in (3.4), we obtain

$$[1 - \epsilon(\gamma - 1)\phi_t]\phi_{xx} - \phi_{tt} = 2\epsilon\phi_x\phi_{tx}, \quad (3.5)$$

which we refer to as the straightforward WNE.

Despite being the most consistent and most obvious weakly nonlinear approximation, this equation has not received much attention in the literature. In fact, the only work we are aware of that gives the above equation (albeit in its viscous form) is Crighton's 1979 review article (38), where its derivation is attributed to Blackstock. Consequently, it might be more appropriate to call (3.5) the inviscid Blackstock–Crighton equation.

3.2 The inviscid Kuznetsov equation

A slightly different weakly nonlinear model is attributed to Kuznetsov (3, 6, 8). The lossless version of the latter reads

$$\phi_{xx} - [1 + \epsilon(\gamma - 1)\phi_t]\phi_{tt} = 2\epsilon\phi_x\phi_{xt}, \quad (3.6)$$

which we refer to as the IKE. Clearly, the IKE and the WNE are both valid weakly nonlinear approximations to (3.4) of the same asymptotic order of approximation with respect to the small parameter ϵ . However, it is important to realize that, although the IKE and the WNE look similar, they are not identical. Clearly, Kuznetsov employed additional approximations that were not reported in his paper (see the passage from (13) to (14) in (8)), where the claim is made that (3.6) follows directly from the approximate (weakly nonlinear) equation of state. Other authors (see, for example, (3) and the references therein) make use of approximate relations between the primitive variables and the potential function to obtain this equation.

The IKE can be derived rigorously from the PEE (10), or the WNE, by multiplying both sides of (3.4), or (3.5), by $[1 - \epsilon(\gamma - 1)\phi_t]^{-1}$, expanding the latter in a binomial series (assuming $\epsilon \ll 1$ is sufficiently small), and then neglecting terms that are $\mathcal{O}(\epsilon^2)$. While this yields a somewhat simpler equation than (3.4), it offers no advantage with regard to obtaining an analytical solution. In fact, from the physical point of view the use of a binomial expansion is unnecessary and should be avoided. As we will show, the WNE is, indeed, a better approximation than the IKE.

3.3 The Lighthill–Westervelt equation

Another popular weakly nonlinear approximation can be obtained by employing the LIA $\phi_x \approx -\phi_t$ (3, 6, 10) only on the right-hand (that is, the perturbing) side of (3.6). This yields

$$\phi_{xx} - [1 + \epsilon(\gamma + 1)\phi_t]\phi_{tt} = 0, \quad (3.7)$$

which we refer to as the LWE.

In essence, the LIA claims that the pressure/density and velocity are in phase. It is strictly valid (and exact) for linear progressive waves. For nonlinear waves, the LIA is a valid approximation only in the immediate vicinity of the wave-front. Making use of the LIA removes the mixed derivative term ϕ_{xt} from the equation of motion. Hence, from a mathematical point of view, this is regarded as a desirable simplification since it yields an equation that is more amenable to standard analytical and numerical methods. However, as we have shown in (11), there is no justifiable physical reason to employ the LIA since it gives rise to a model that is seriously crippled.

It should be noted that the original derivation of (3.7) is attributed to Westervelt (3, 6, 9), who used the celebrated Lighthill turbulence stress tensor for the acoustic field (39), in the context of parametric acoustic arrays (9) and the scattering of sound by sound (40). Thus, the original derivation and its context are rather different from the now-common approach of deriving the LWE as a weakly nonlinear approximation to (3.4) via the IKE and the LIA. In fact, it appears that Westervelt employed a number of approximations without due justification. We prefer to think of the LWE as a further approximation stemming from the IKE. This is especially helpful when trying to understand why the LWE performs significantly worse than its siblings, the IKE and the WNE.

4. Reformulation of the potential equations as conservation laws

In order to ascertain the range of applicability of the approximate models, one has to be able to numerically solve the corresponding equations not only when the solution is smooth but also after the instant of shock formation. It is well known that equations whose solutions develop singularities in finite time are very difficult to solve numerically. However, in the past couple of decades Godunov-type schemes have proved to be adequate tools for solving hyperbolic systems of conservation laws (12, 13) that admit discontinuous solutions. Therefore, to use the latter numerical methods, we must

reformulate our models as conservation laws. In this section, we proceed to show how this can be done.

It is easy to see that (3.1), (3.2) and (3.3) can be written as the following conservation law:

$$\begin{pmatrix} \rho \\ \rho u \end{pmatrix}_t + \begin{pmatrix} \epsilon \rho u \\ \epsilon \rho u^2 + \epsilon^{-1} \rho^\gamma / \gamma \end{pmatrix}_x = 0, \tag{4.1}$$

by adding (3.1) multiplied by u to (3.2) and eliminating the pressure from the latter via (3.3).

For the WNE, however, the first step is to rewrite (3.5) as a first-order system of equations. Hence, let us recall the following relations (10, 11, 16):

$$\begin{aligned} \phi_x &= u, \\ \phi_t &= \epsilon^{-1}(1 - \rho). \end{aligned} \tag{4.2}$$

Employing the latter we obtain the following first-order system of equations:

$$\begin{aligned} \left[\rho - \frac{1}{2} \epsilon^2 (3 - \gamma) u^2 \right]_t + \epsilon \{ [1 - (\gamma - 1)(1 - \rho)] u \}_x &= 0, \\ u_t + \epsilon^{-1} \rho_x &= 0. \end{aligned} \tag{4.3}$$

Now, we introduce the variable transformation

$$\tilde{\rho} \stackrel{\text{def}}{=} \rho - \frac{1}{2} (3 - \gamma) \epsilon^2 u^2 \iff \rho = \tilde{\rho} + \frac{1}{2} (3 - \gamma) \epsilon^2 u^2, \tag{4.4}$$

which, upon substitution into (4.3), results in the following conservation law for the WNE:

$$\begin{pmatrix} \tilde{\rho} \\ u \end{pmatrix}_t + \begin{pmatrix} \epsilon \{ 1 - (\gamma - 1) [1 - \tilde{\rho} - \frac{1}{2} (3 - \gamma) \epsilon^2 u^2] \} u \\ \epsilon^{-1} \tilde{\rho} + \frac{1}{2} (3 - \gamma) \epsilon u^2 \end{pmatrix}_x = 0. \tag{4.5}$$

In a similar fashion, the IKE, given by (3.6), can be recast as the first-order system

$$\begin{aligned} \left[\gamma \rho - \frac{1}{2} (\gamma - 1) \rho^2 - \epsilon^2 u^2 \right]_t + \epsilon u_x &= 0, \\ u_t + \epsilon^{-1} \rho_x &= 0. \end{aligned} \tag{4.6}$$

Then, we introduce the variable transformation

$$\tilde{\rho} \stackrel{\text{def}}{=} \gamma \rho - \frac{1}{2} (\gamma - 1) \rho^2 - \epsilon^2 u^2 \iff \rho = \frac{1}{\gamma - 1} \left[\gamma \mp \sqrt{\gamma^2 - 2(\gamma - 1)(\epsilon^2 u^2 + \tilde{\rho})} \right], \tag{4.7}$$

where the minus sign must be selected because we require that $\tilde{\rho} \rightarrow 0$ as $\rho, u \rightarrow 0$. Upon substituting the latter into (4.6), we find that the conservation law corresponding to the IKE is

$$\begin{pmatrix} \tilde{\rho} \\ u \end{pmatrix}_t + \begin{pmatrix} \epsilon u \\ -[\epsilon(\gamma - 1)]^{-1} \sqrt{\gamma^2 - 2(\gamma - 1)(\epsilon^2 u^2 + \tilde{\rho})} \end{pmatrix}_x = 0. \tag{4.8}$$

Again, using the identities in (4.2), the LWE, given by (3.7), can be written as the following first-order system of partial differential equations:

$$\begin{aligned} \left[(\gamma + 2)\varrho - \frac{1}{2}(\gamma + 1)\varrho^2 \right]_t + \epsilon u_x &= 0, \\ u_t + \epsilon^{-1}\varrho_x &= 0. \end{aligned} \tag{4.9}$$

Then, we introduce the variable transformation

$$\tilde{\varrho} \stackrel{\text{def}}{=} (\gamma + 2)\varrho - \frac{1}{2}(\gamma + 1)\varrho^2 \iff \varrho = \frac{1}{\gamma + 1} \left[\gamma + 2 \mp \sqrt{(\gamma + 2)^2 - 2(\gamma + 1)\tilde{\varrho}} \right], \tag{4.10}$$

where, again, the minus sign must be selected because we require that $\tilde{\varrho} \rightarrow 0$ as $\varrho, u \rightarrow 0$. Upon substituting the latter into (4.9), we find that the conservation law corresponding to the LWE is

$$\begin{pmatrix} \tilde{\varrho} \\ u \end{pmatrix}_t + \begin{pmatrix} \epsilon u \\ -[\epsilon(\gamma + 1)]^{-1} \sqrt{(\gamma + 2)^2 - 2(\gamma + 1)\tilde{\varrho}} \end{pmatrix}_x = 0. \tag{4.11}$$

Henceforth, in order to avoid ambiguity, we refer to the conservation law reformulations of the model equations derived in this section, that is, (4.1), (4.5), (4.8) and (4.11), as the Euler equations conservation law (EECL), the weakly nonlinear conservation law (WNCL), the inviscid Kuznetsov conservation law (IKCL) and the Lighthill–Westervelt conservation law (LWCL), respectively.

5. What makes one weakly nonlinear model better than another?

In this section, we give an argument, based on the first-order system formulation of the model equations, of why the LWE performs significantly worse than the IKE and WNE, and why the WNE is the ‘truly consistent’ weakly nonlinear model.

From the theory of characteristics (41), we know that a nonlinear acoustic wave has an amplitude-dependent propagation speed. That is, a fluid particle of certain density and velocity moves in space with a speed determined by the corresponding eigenvalue of the system of equations, which may depend on the density and velocity of said fluid particle. Therefore, we must analyse the structure of the first-order system formulation of the approximate equations to gain insight into the behavior of their (nonlinear wave) solutions.

To this end, after some algebraic manipulations, the WNE system, given in (4.3), can be rewritten as

$$\begin{pmatrix} \varrho \\ u \end{pmatrix}_t + \begin{pmatrix} 2\epsilon u & \epsilon[1 - (\gamma - 1)(1 - \varrho)] \\ \epsilon^{-1} & 0 \end{pmatrix} \begin{pmatrix} \varrho \\ u \end{pmatrix}_x = 0, \tag{5.1}$$

and we find that the eigenvalues of the coefficient matrix are

$$\lambda_{1,2} = \epsilon u \pm \sqrt{\epsilon^2 u^2 + (\gamma - 1)\varrho + 2 - \gamma}. \tag{5.2}$$

Since the square-root function is positive and monotone, we have that $\lambda_1 \neq \lambda_2$ and $\lambda_{1,2} \in \mathbb{R}$ for all $t \geq 0$, as long as its argument remains non-negative, that is,

$$\gamma - 2 < (\gamma - 1)\varrho + \epsilon^2 u^2 \implies \varrho > (\gamma - 2)/(\gamma - 1) + \mathcal{O}(\epsilon^2); \tag{5.3}$$

this gives an upper limit of validity for the WNE. However, it is important to notice here that, since $\varrho > 0$, the bound in (5.3) is always satisfied. Hence, no matter how large ϱ is, (5.1) is strictly hyperbolic (and thus remains valid) provided $\gamma \leq 2$, which is always true for gases (1, 2).

Similarly, the IKE system, given in (4.6), can be recast as

$$\begin{pmatrix} \varrho \\ u \end{pmatrix}_t + \begin{pmatrix} \frac{2\epsilon u}{\gamma - (\gamma - 1)\varrho} & \frac{\epsilon}{\gamma - (\gamma - 1)\varrho} \\ \epsilon^{-1} & 0 \end{pmatrix} \begin{pmatrix} \varrho \\ u \end{pmatrix}_x = 0, \tag{5.4}$$

and we find that the eigenvalues of the coefficient matrix are

$$\lambda_{1,2} = \frac{\epsilon u \pm \sqrt{\epsilon^2 u^2 + \gamma - (\gamma - 1)\varrho}}{\gamma - (\gamma - 1)\varrho}. \tag{5.5}$$

As before, we have that $\lambda_1 \neq \lambda_2$ and $\lambda_{1,2} \in \mathbb{R}$ for all $t \geq 0$, as long as the argument of the square root remains non-negative, that is,

$$(\gamma - 1)\varrho < \epsilon^2 u^2 + \gamma \implies \varrho < \gamma / (\gamma - 1) + \mathcal{O}(\epsilon^2); \tag{5.6}$$

this gives an upper limit of validity for the IKE.

Also, the LWE system, given in (4.9), can be re-expressed as

$$\begin{pmatrix} \varrho \\ u \end{pmatrix}_t + \begin{pmatrix} 0 & \frac{\epsilon}{\gamma + 2 - (\gamma + 1)\varrho} \\ \epsilon^{-1} & 0 \end{pmatrix} \begin{pmatrix} \varrho \\ u \end{pmatrix}_x = 0, \tag{5.7}$$

and we find that the eigenvalues of the coefficient matrix are

$$\lambda_{1,2} = \frac{\pm 1}{\sqrt{\gamma + 2 - (\gamma + 1)\varrho}}. \tag{5.8}$$

Again, $\lambda_1 \neq \lambda_2$ and $\lambda_{1,2} \in \mathbb{R}$ for all $t \geq 0$, as long as the argument of the square root in the denominator remains positive, that is,

$$(\gamma + 1)\varrho < \gamma + 2 \implies \varrho < (\gamma + 2) / (\gamma + 1). \tag{5.9}$$

Consequently, the LWE is strictly hyperbolic only when the latter inequality is satisfied.

Here, it is important to note that the WNE has the least restrictive requirement (in fact, one that is always satisfied for gases) on the value of the density that makes the corresponding first-order system strictly hyperbolic. On the other hand, both the IKE and the LWE have more restrictive upper bounds. Therefore, even for not-so-weakly nonlinear waves, we can expect that out of the three approximate equations considered in this paper, the solutions of the WNE will remain the closest to the exact ones (that is, those of the Euler equations). However, as long as the physical setup is within the limits of the finite-amplitude approximation (small ϱ), all the aforementioned bounds on the density are satisfied.

Moreover, the eigenvalues of the WNE and IKE systems given in (5.2) and (5.5), respectively, depend upon the density and the velocity; therefore, there is a built-in balancing process. Similarly, if we examine the IKCL and LWCL, given in (4.8) and (4.11), respectively, we realize that they are almost identical, except that the second component of the flux vector of the IKCL contains a term proportional to $-u^2$. Consequently, the flux of the second conserved variable is always less than the corresponding flux in the LWCL. Therefore, we can deduce that the lack of this ‘balancing term’ in the LWCL can lead to the premature steepening and breaking of the wave, as we will see in section 6, when a velocity boundary condition (BC) is prescribed.

6. Numerical results

In (10), we considered the model equations subject only to a BC on the density. Though the latter provides a good context in which to study the weakly nonlinear models, it is less realistic than a BC on the velocity. That is to say, the density BC is more difficult to implement in real, physical situations, while a velocity BC is natural when studying, for example, the motion of pistons. Moreover, we have shown in (11) that the velocity BC proves to be ‘more challenging’ for the approximate models. Therefore, it is important to study the performance of the model equations in the context of both types of BCs, and we do so in this section.

To this end, we consider the conservation laws derived in section 4, that is, the EECL, WNCL, IKCL and LWCL, subject to the initial conditions

$$\rho(x, 0) = 0, \quad u(x, 0) = 0, \quad (6.1)$$

and the BCs

$$\left\{ \begin{array}{l} \text{(density BC)} \quad \rho(0, t) \\ \text{(velocity BC)} \quad \epsilon u(0, t) \end{array} \right\} = [H(t) - H(t - t_w)]f(t), \quad (6.2)$$

where $H(\cdot)$ denotes the Heaviside unit step function, and recall that $\rho \equiv \varrho - 1$ denotes the dimensionless acoustic density (or condensation). Note that the first two conditions reflect the fact that the medium ahead of wave-front Σ is in its equilibrium state, and the third means that a pulse of finite duration (or width) t_w is introduced at the $x = 0$ boundary at time $t = 0^+$. For the simulations below, we take $t_w = 1$, $f(t) = \epsilon \sin(\pi t)$, $\epsilon = 0.26503$ and the medium to be air at 20°C ($\Rightarrow \gamma = 1.4$). Moreover, the spatial interval on which the equations are solved is chosen to be large enough so that no reflections occur from the downstream boundary. Finally, we note that for these parameter values, and for both the density and the velocity BCs, the predicted blow-up time of the acceleration wave’s amplitude is $t_\infty = 1$; see Appendix B.

6.1 Comparison of the solution profiles

We begin with the comparison of the solutions of the four models prior to the blow-up time t_∞ . In Figs 1 to 5, we have plotted the solution of the EECL in blue, the WNCL in magenta, the IKCL in green and the LWCL in red; the dashed black line is the solution to the linear wave equation, and the solid black line is the theoretical slope of the curve at the wave-front (see (B.7)). The top row of each collection of plots shows the results for the density BC, and the bottom row shows the results for the velocity BC.

From Fig. 1, it is clear that, even for times much before the instant of blow-up, the solutions of the WNCL and IKCL are very close to the solution of the EECL, while the solution of the LWCL is not. Moreover, the profiles predicted by the WNCL are always closer to the EECL than those predicted by the IKCL. This shows that the unnecessary approximations made in deriving the IKE and LWE degrade the performance of these models. In addition, it should be noted that the difference between the solutions of the WNCL and IKCL appears to be of order $\epsilon^2 \approx 0.07$, at least for $t \ll t_\infty$, which is quantitatively fully consistent with the approximations we have made.

As discussed in (10), a weakly nonlinear approximation can eventually lead to a faster steepening of the profile because of the saturation of the nonlinearity. This is due to the fact that (3.4) contains a term cubic in ϕ , which the approximate equations lack, that can mitigate the adverse effects of the term quadratic in ϕ , when the gradients of the potential become considerably large. The saturation

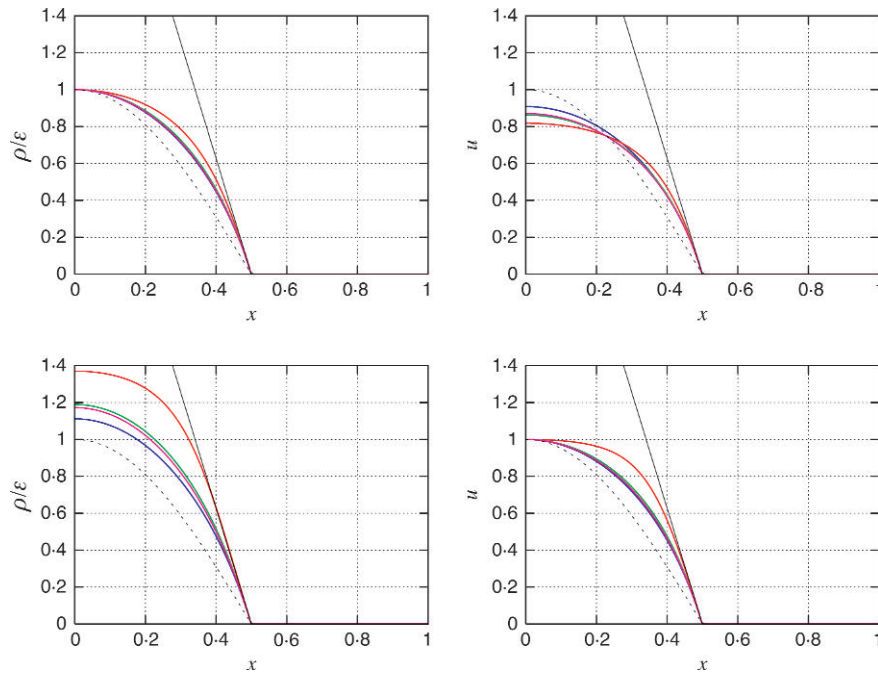


Fig. 1 Snapshots of the scaled dimensionless acoustic density ρ/ϵ and velocity u at $t = 0.5$. In the top and bottom row of each collection of plots are the results for the density and velocity BCs, respectively. The color convention is as follows: in blue is the EECL, in magenta is the WNCL, in green is the IKCL, in red is the LWCL, in dashed black is the linear wave equation and in solid black is the theoretical tangent at the wave-front

of the nonlinearity is enhanced in the IKCL and LWCL, whose solutions steepen faster than that of the WNCL, resulting in a larger deviation from that of the EECL, as shown particularly well by Figs 2 and 3. Furthermore, the numerical results shown in the latter figures suggest that the velocity BC triggers a faster response from the nonlinear terms than the density BC, thus the solutions of the WNCL and IKCL end up more than twice the distance from the reference (EECL) solution as compared with the density BC case.

The important result here is that the profiles predicted by the WNCL are in very good quantitative agreement with the corresponding exact (EECL) profiles, while the profiles predicted by the IKCL and LWCL are not. In particular, the solution of the LWCL appears to break prematurely by/at $t = 0.75$ in the case of the velocity BC (see the bottom row of Fig. 2)! The formation of a shock before the blow-up time of the acceleration wave, as predicted by singular surface theory, means that the mechanisms of wave steepening (that is, the cumulative effects of nonlinearity) in the LWCL operate at a faster rate than in the other models.

Figure 3 shows the situation at the instant of blow-up, that is, $t = t_\infty$. The solutions of the WNCL and IKCL follow strictly the steepening pattern of the exact (EECL) solution. Though the amplitude of the wave is slightly exaggerated, the slope of the numerical solution at the wave-front is in very good agreement with that of the theoretical tangent line (see (B.7)), which is exactly vertical in this case. The LWCL again demonstrates an incorrect steepening mechanism; in the case of the

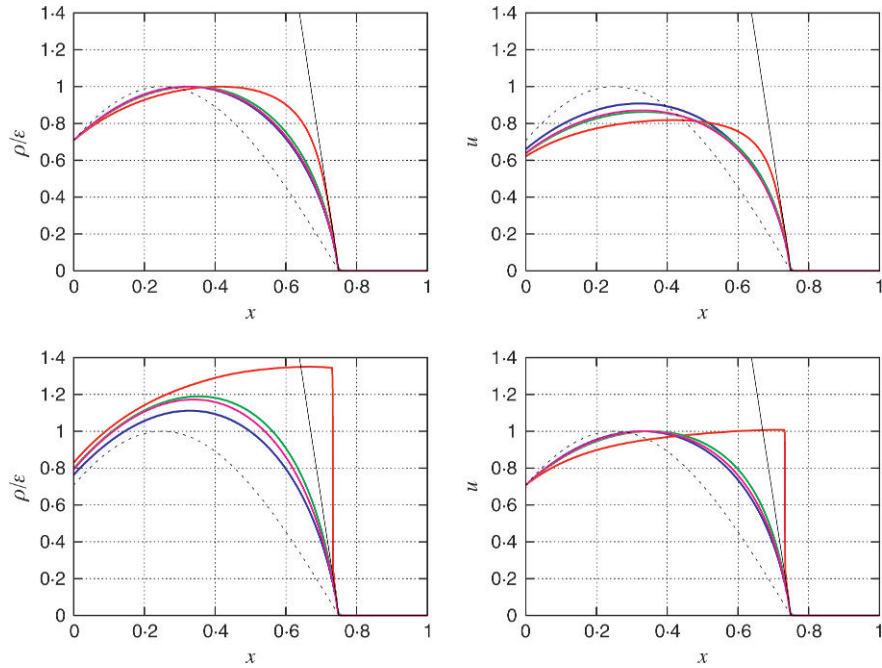


Fig. 2 Snapshots of the scaled dimensionless acoustic density ρ/ϵ and velocity u at $t = 0.75$ for the density BC (top row) and the velocity BC (bottom row). The color convention is the same as in Fig. 1

velocity BC, the solution has advanced beyond the wave-front and is considerably different from the reference one since it appears to have already formed a shock by/at $t = 0.75$.

Figure 3 also illustrates the following interesting result. If the LWCL profile in both the upper panels were replaced with the one from the lower left panel, then the ‘transplanted’ LWCL profile would be in closer agreement (near $x \approx 0.4$) with the existing EECL, WNCL and IKCL profiles, for both the density and the velocity. This observation serves to highlight the extent to which the qualitative behavior of the solution changes when terms containing different partial derivatives are swapped. Since, in the derivation of the LWE, a term proportional to the velocity (that is, ϕ_x) was replaced by a term proportional to the density (that is, ϕ_t), then imposing the BC on the velocity makes the latter behave similarly to the density in the other models when a density BC is imposed. In a sense, the LWE does not correctly ‘recognize’ the physical quantity called velocity. All this means that the LWE presents a distorted physical picture and should not be used for actual modeling of acoustic wave propagation.

Figures 4 and 5 show that the same observations are true for times beyond the instant of blow-up. At this point, the WNCL and IKCL show an, albeit small, increase in the speed of the shock wave, while the LWCL is completely wrong. The faster (compared to the EECL) shock speed predicted by the approximate models can be explained by invoking the Rankine–Hugoniot conditions (12, 13, 41), appropriately formulated for the conservation laws derived in section 4. In other words, the saturation of the nonlinearity in the approximate models results in excessive steepening of the wave-form; and thus, the amplitude of the shock wave (when it forms) is larger for the latter than for

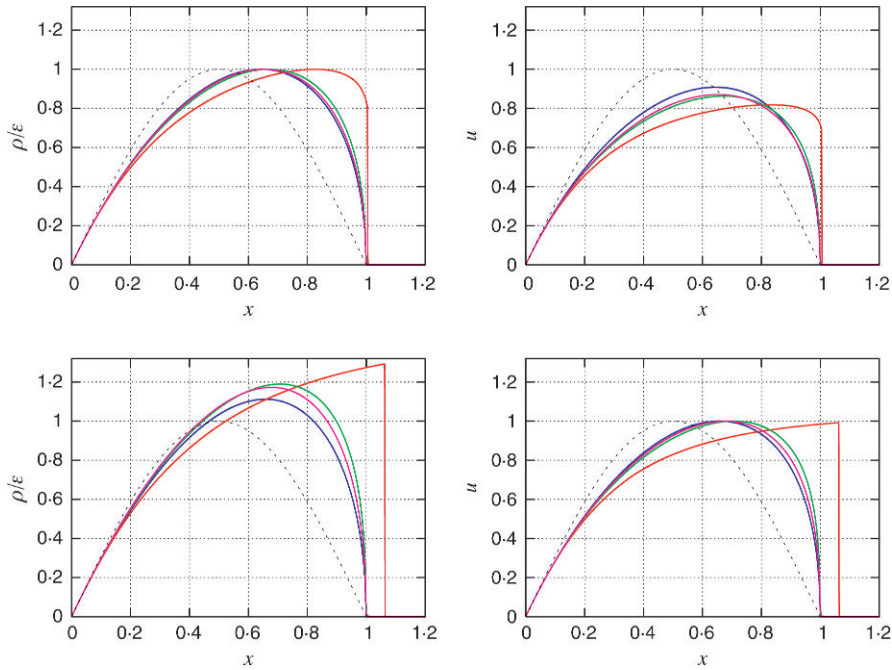


Fig. 3 Snapshots of the scaled dimensionless acoustic density ρ/ϵ and velocity u at $t = 1.0$ for the density BC (top row) and the velocity BC (bottom row). The color convention is the same as in Fig. 1

the EECL. Therefore, the discontinuity propagates faster than predicted by the EECL. Furthermore, in the vicinity of the shock, the solution of the WNCL is closer to that of the EECL than the solution of the IKCL. Consequently, it is clear that, in the context of finite-amplitude acoustics, the WNE is a better choice than the IKE. Of course, this should not be a surprise; as we have already mentioned, the IKE embodies an additional (unnecessary) approximation.

6.2 Quantifying the error in the approximate equations

Following the same color convention established in Fig. 1, in the left column of Fig. 6 we have plotted the L^1 -norm of the difference between each of the approximate solutions (that is, those of the WNCL, IKCL and LWCL) and the reference (EECL) solution, as a function of time, for the density. That is to say, we plot the quantity

$$\mathcal{L}^1_{\text{error}}(t) = \frac{1}{N} \sum_{i=0}^{N-1} |\varrho_{\text{approx}}(x_i, t) - \varrho_{\text{exact}}(x_i, t)|, \tag{6.3}$$

where N is the number of computational cells used and x_i is the center of each one (see Appendix A). Even past the blow-up time of the acceleration wave (or shock formation), the latter quantity is a good measure of the error because the weak solutions to the conservation laws (that is, shocks) are no longer continuous functions but only integrable (that is, L^1) functions (13). Note

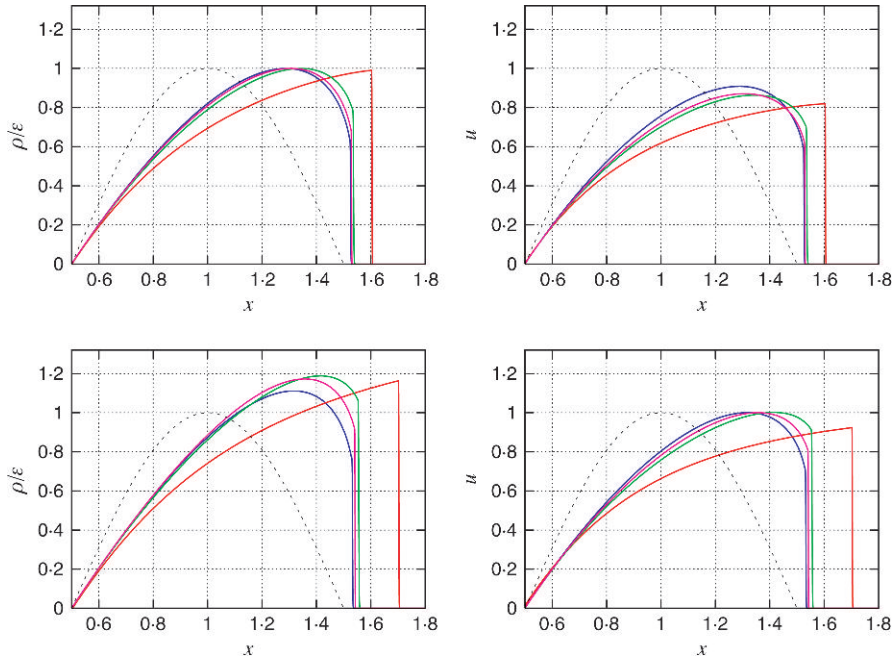


Fig. 4 Snapshots of the scaled dimensionless acoustic density ρ/ϵ and velocity u at $t = 1.5$ for the density BC (top row) and the velocity BC (bottom row). The color convention is the same as in Fig. 1

that q_{exact} stands for the numerical solution to the EECL and not an analytical exact solution to the initial-boundary value problem.

The trend of the error curves is similar for the two types of BCs we considered. There is a saturation of the error with time, which correlates with the fact that the profiles of the solutions eventually ‘break’ due to a combination of nonlinear steepening and blow-up of the acceleration wave, at which point the profiles no longer change rapidly in time. In other words, as the steepening occurs initially, we see the rapid error growth, thereafter the error’s order of magnitude is more or less constant. The most important result (see also (11)) is that the LWCL error is consistently an order of magnitude larger than the IKCL error, which further exemplifies the inadequacy of the LIA for nonlinear waves. Moreover, the WNCL error is, on average, half an order of magnitude smaller for the density BC and a third of an order of magnitude smaller for the velocity BC than the respective IKCL error. This shows that the WNE is consistently performing better than the IKE and, of course, the LWE.

Furthermore, in the right column of Fig. 6, we have plotted the maximal percent error between the approximate solutions and the reference solution. The latter quantity is defined as

$$\mathcal{P}_{\text{error}}(t) = \max_{0 \leq i \leq N-1} \left| \frac{q_{\text{approx}}(x_i, t) - q_{\text{exact}}(x_i, t)}{q_{\text{exact}}(x_i, t)} \right| \times 100. \quad (6.4)$$

Naturally, it is only well defined up to the moment of blow-up (or shock formation) since it presupposes the solution has meaningful point values (13).

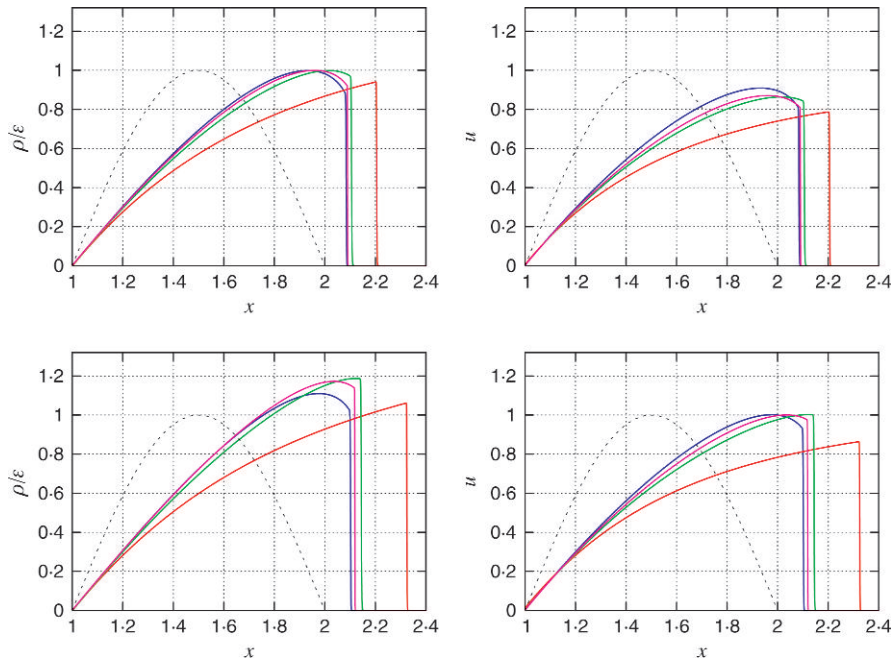


Fig. 5 Snapshots of the scaled dimensionless acoustic density ρ/ϵ and velocity u at $t = 2.0$ for the density BC (top row) and the velocity BC (bottom row). The color convention is the same as in Fig. 1

The maximal error of the LWCL solution is as much as 20 per cent, which corroborates the results in the literature (11, 14), while that of the WNCL and IKCL solutions is less than one per cent and two per cent, respectively. What is important to note is that at the time of shock formation, the maximal percent error in the solution to the WNCL is half that of the IKCL, for both the density and the velocity BCs, showing once again that the WNE consistently performs better than the IKE.

Finally, so as not to belabor the point, we have only shown the error in the density, since the trend of the error in the velocity is similar.

7. Conclusions

In this paper, we have presented an in-depth comparative study of four different models of lossless, nonlinear acoustic propagation: the (exact) Euler equations, a straightforward weakly nonlinear equation (WNE), the inviscid version of Kuznetsov's equation (IKE) and the Lighthill–Westervelt equation (LWE). Upon applying the further assumption, beyond those on the fluid/flow, that $\epsilon \ll 1$, we obtained the WNE from the Euler equations as a finite-amplitude, or weakly nonlinear, approximation. Then, we showed how the IKE and LWE can be derived from the WNE under further approximations. Using this unified framework of the model equations, we have provided a critical discussion of the adequacy and utility of the various 'standard' approximations.

Furthermore, we presented a novel reformulation of the three weakly nonlinear models as hyperbolic systems of conservation laws, which allowed us to employ a Godunov-type finite-difference

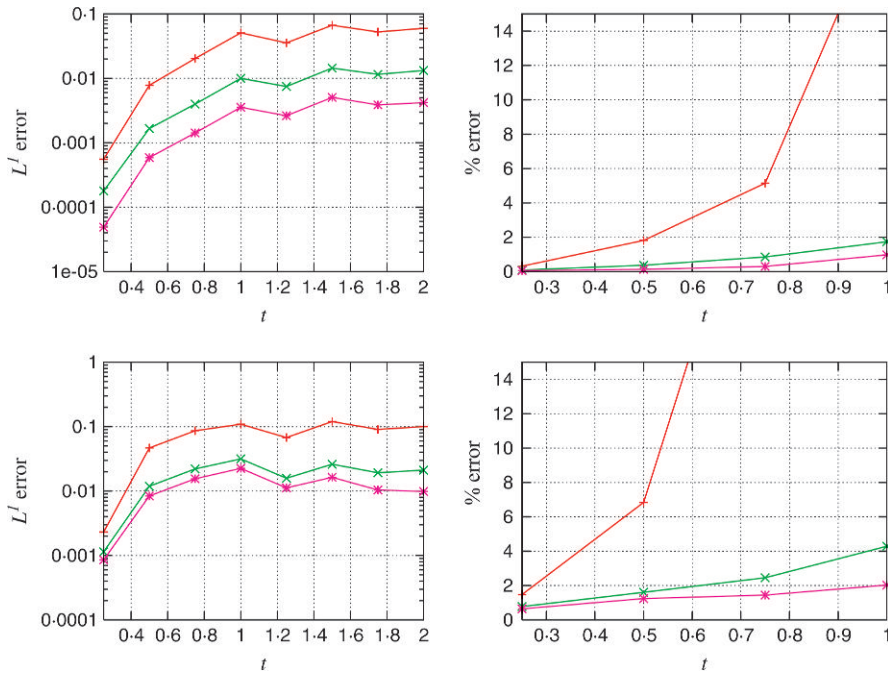


Fig. 6 Growth of the logarithm of the L^1 -norm of the error (left column) and the maximal percent error (right column) in ϱ as functions of time. The top and bottom rows represent the errors for the density and velocity BC, respectively. The color convention is the same as in Fig. 1

scheme to numerically solve the three model equations. In this manner, we obtained (expounding on our previous work (11)) numerical solutions for the WNEs for times exceeding the instant of blow-up (or shock formation). This gave us the unique opportunity to subject the approximate models to rigorous ‘interrogation’ and to ascertain the limits of their validity.

The main result of the present work is that the WNE is, both quantitatively and qualitatively, a much better model (that is, it performs better for longer times and larger Mach numbers) of acoustic waves in lossless fluids than its siblings: the IKE and the LWE. This extends our previous result (11) to include the WNE, namely, we show that, while the WNE’s and IKE’s solutions remain close to the reference one (Euler), the LWE’s does not since the latter model is ‘crippled’ by use of the LIA, giving acceptable results only for $t \ll t_\infty$ and $\epsilon \ll 1$.

A far-reaching conclusion of this paper (supporting our previous ones (10, 11)) is that cumulative nonlinear effects, such as nonlinear steepening, are significantly affected by the assumptions made in the weakly nonlinear approximations. That is to say, even though (as testified by the singular surface theory analysis) the dynamics at the wave-front are identical in the approximate and exact equations (when the medium ahead of the wave-front is in its equilibrium state), the cumulative effects of nonlinearity can lead to steepening and even breaking (shock formation) behind the wave-front (recall the bottom row of Fig. 2). It was only possible to discover the latter effects after reformulating the model equations as conservation laws and using the powerful numerical tool of Godunov-type schemes.

Another important finding was that the cubic nonlinearity in the PEE (that is, (2.18) and (3.4)) plays a crucial role in the development of a wave-form. In particular, even though the cubic term is an order of magnitude smaller in ϵ than the quadratic term, neglecting the former can noticeably alter the long-time dynamics because it ‘saturates’ the nonlinearity. That is to say, the cubic term tends to limit the nonlinear steepening of the wave because it has the opposite sign from the quadratic term, mitigating the adverse effects of the latter. For this reason, all three weakly nonlinear models tend to artificially amplify the cumulative nonlinear effects.

Finally, we note that future work could include studying (2.24) the exact potential equation for a barotropic fluid with a quadratic equation of state, which involves the Lambert W -function, that we derived in section 2.2. In addition, one could extend the present approach of deriving consistent weakly nonlinear approximations, and providing numerical results via Godunov-type schemes, to non-homentropic flows (42) and/or to the modern theories of gas dynamics (24).

Acknowledgments

We would like to thank the two referees for their valuable suggestions and comments. C.I.C. was supported, in part, by an ASEE/ONR Summer Senior Faculty Fellowship at the U.S. Naval Research Laboratory, Stennis Space Center, Mississippi. P.M.J. was supported by ONR/NRL funding (PE 061153N). All figures appearing in this article were generated using the software package GNUPLOT (version 4.0).

References

1. P. A. Thompson, *Compressible-Fluid Dynamics* (McGraw–Hill, New York 1972).
2. L. I. Sedov, *Mechanics of Continuous Media* (World Scientific, River Edge, NJ 1997), Chapter 8.
3. K. Naugolnykh and L. Ostrovsky, *Nonlinear Wave Processes in Acoustics* (Cambridge University Press, New York 1998), Chapter 1.
4. M. F. Hamilton and C. L. Morfey, Model equations, *Nonlinear Acoustics: Theory and Applications* (ed. M. F. Hamilton & D. T. Blackstock; Academic Press, New York 1997) 41–63.
5. S. Makarov and M. Ochmann, Nonlinear and thermoviscous phenomena in acoustics, Part I, *Acoustica* **82** (1996) 579–606.
6. S. Makarov and M. Ochmann, Nonlinear and thermoviscous phenomena in acoustics, Part II, *ibid.* **83** (1997) 197–222.
7. S. Makarov and M. Ochmann, Nonlinear and thermoviscous phenomena in acoustics, Part III, *ibid.* **83** (1997) 827–846.
8. V. P. Kuznetsov, Equations of nonlinear acoustics, *Sov. Phys. Acoust.* **16** (1971) 467–470.
9. P. J. Westervelt, Parametric acoustic array, *J. Acoust. Soc. Amer.* **35** (1963) 535–537.
10. I. Christov, P. M. Jordan and C. I. Christov, Nonlinear acoustic propagation in homentropic perfect gases: a numerical study, *Phys. Lett. A* **353** (2006) 273–280.
11. I. Christov, C. I. Christov and P. M. Jordan, Cumulative nonlinear effects in acoustic wave propagation, *Comput. Model. Engng Sci.* **17** (2007) 47–54.
12. E. R. Toro, *Riemann Solvers and Numerical Methods for Fluid Dynamics* (Springer, Berlin 1999).

13. R. J. LeVeque, *Finite Volume Methods for Hyperbolic Problems* (Cambridge University Press, New York 2002).
14. Y. Kagawa, T. Tsuchiya, T. Yamabuchi, H. Kawabe and T. Fuji, Finite element simulation of non-linear sound wave propagation, *J. Sound Vib.* **154** (1992) 125–145.
15. T. Tsuchiya and Y. Kagawa, A simulation study on nonlinear sound propagation by a finite element approach, *J. Acoust. Soc. Jpn* (E) **13** (1992) 223–230.
16. P. M. Jordan and C. I. Christov, A simple finite-difference scheme for modeling the finite-time blow-up of acoustic acceleration waves, *J. Sound Vib.* **281** (2005) 1207–1216.
17. Y. Inoue and T. Yano, Propagation of strongly nonlinear plane N -waves, *J. Fluid Mech.* **341** (1997) 59–76.
18. T. R. Fogarty and R. J. LeVeque, High-resolution finite-volume methods for acoustic waves in periodic and random media, *J. Acoust. Soc. Amer.* **106** (1999) 17–28.
19. P. J. Chen, Growth and decay of waves in solids, *Handbuch der Physik*, Vol. VIa/3 (ed. S. Flügge & C. Truesdell; Springer, Berlin 1973) 303–402.
20. B. D. Coleman and M. E. Gurtin, Growth and decay of discontinuities in fluids with internal state variables, *Phys. Fluids* **10** (1967) 1454–1458.
21. Y. B. Fu and N. H. Scott, The transition from acceleration wave to shock wave, *Int. J. Engng Sci.* **29** (1991) 617–624.
22. T. Y. Thomas, The growth and decay of sonic discontinuities in ideal gases, *J. Math. Mech.* **6** (1957) 455–469.
23. A. R. Elcrat, On the propagation of sonic discontinuities in the unsteady flow of a perfect gas, *Int. J. Engng Sci.* **15** (1977) 29–34.
24. P. M. Jordan and B. Straughan, Acoustic acceleration waves in homentropic Green and Naghdi gases, *Proc. R. Soc. A* **462** (2006) 3601–3611.
25. M. F. McCarthy, Singular surfaces and waves, *Continuum Physics*, Vol. II (ed. A. C. Eringen; Academic Press, London 1975) 449–521.
26. K. A. Lindsay and B. Straughan, Acceleration waves and second sound in a perfect fluid, *Arch. Ration. Mech. Anal.* **68** (1978) 53–87.
27. B. Straughan, Nonlinear waves in a general magnetic fluid, *J. Appl. Math. Phys.* **37** (1986) 274–279.
28. G. Saccomandi, Acceleration waves in a thermo-microstretch fluid, *Int. J. Non-Linear Mech.* **29** (1994) 809–817.
29. M. Ostoja-Starzewski and J. Trębicki, On the growth and decay of acceleration waves in random media, *Proc. R. Soc. A* **455** (1999) 2577–2614.
30. R. Quintanilla and B. Straughan, A note on discontinuity waves in type III thermoelasticity, *ibid.* **460** (2004) 1169–1175.
31. P. M. Jordan, Growth and decay of acoustic acceleration waves in Darcy-type porous media, *ibid.* **461** (2005) 2749–2766.
32. A. Morro, Jump relations and discontinuity waves in conductors with memory, *Math. Comput. Model.* **43** (2006) 138–149.
33. M. Ciarletta and B. Straughan, Thermo-poroacoustic acceleration waves in elastic materials with voids, *J. Math. Anal. Appl.* **333** (2007) 142–150.
34. J. Jaisaardsuetrong and B. Straughan, Thermal waves in a rigid heat conductor, *Phys. Lett. A* **366** (2007) 433–436.
35. R. M. Corless, G. H. Gonnet, D. E. G. Hare, D. J. Jeffrey and D. E. Knuth, On the Lambert W function, *Adv. Comput. Math.* **5** (1996) 329–359.

36. R. T. Beyer, The parameter B/A , *Nonlinear Acoustics* (ed. M. F. Hamilton & D. T. Blackstock; Academic Press, New York 1997) 25–39.
37. H. Ockendon and J. R. Ockendon, Nonlinearity in fluid resonances, *Meccanica* **36** (2001) 297–321.
38. D. G. Crighton, Model equations of nonlinear acoustics, *Ann. Rev. Fluid Mech.* **11** (1979) 11–33.
39. M. J. Lighthill, On sound generated aerodynamically. I. General theory, *Proc. R. Soc. A* **211** (1952) 564–587.
40. H. C. Woodsum and P. J. Westervelt, A general theory for the scattering of sound by sound, *J. Sound Vib.* **76** (1981) 179–186.
41. G. B. Whitham, *Linear and Nonlinear Waves* (Wiley-Interscience, New York 1974).
42. H. Lin and A. J. Szeri, Shock formation in the presence of entropy gradients, *J. Fluid Mech.* **431** (2001) 161–188.
43. A. Harten, P. D. Lax and B. van Leer, On upstream differencing and Godunov-type schemes for hyperbolic conservation laws, *SIAM Rev.* **25** (1983) 35–61.
44. C. Truesdell and K. R. Rajagopal, *An Introduction to the Mechanics of Fluids* (Birkhäuser, Boston 2000), Chapter 11.
45. D. R. Bland, *Wave Theory and Applications* (Oxford University Press, Oxford 1988).

APPENDIX A

The high-resolution Godunov-type conservative numerical method that we used to numerically solve the conservation law discussed in section 4 is known as the MUSCL–Hancock scheme (12), which is an $\mathcal{O}[(\Delta x)^2 + (\Delta t)^2]$ accurate method, in regions of smooth flow. In this Appendix, we present a brief summary of the algorithm.

To this end, consider a generic hyperbolic system of conservation laws:

$$\mathbf{Q}_t + \mathbf{F}(\mathbf{Q})_x = 0, \quad (\text{A.1})$$

where \mathbf{Q} and $\mathbf{F}(\mathbf{Q})$ are column vectors containing the conserved quantities and their corresponding fluxes, respectively. Then, given the domain $[0, l]$, we construct a cell-centered grid with N cells; that is, letting $\Delta x = l/N$, the cells' centers are located at $x_i = (i + \frac{1}{2})\Delta x$, $0 \leq i \leq N - 1$. The average of \mathbf{Q} over the i th cell at time $t = t^n$ (that is, at the n th time step), denoted by \mathbf{Q}_i^n and assigned to be the value of \mathbf{Q} at the cells' centers, is the quantity we seek to compute.

We approximate the conservation law in (A.1) via the conservative discretization

$$\mathbf{Q}_i^{n+1} = \mathbf{Q}_i^n + \frac{\Delta t^n}{\Delta x} \left(\mathbf{F}_{i-\frac{1}{2}}^n - \mathbf{F}_{i+\frac{1}{2}}^n \right), \quad (\text{A.2})$$

where $\mathbf{F}_{i-\frac{1}{2}}^n$ and $\mathbf{F}_{i+\frac{1}{2}}^n$ denote the fluxes through the left and right interface of the i th cell, respectively. Henceforth, we leave the temporal superscript n understood.

Since the discretization given in (A.2) is only first-order accurate in space and time, we perform a slope-limited linear (MUSCL) extrapolation of the cell interface values of \mathbf{Q} based upon the cell center values to obtain second-order accuracy in space. In other words, we choose

$$\mathbf{Q}_i^{\text{L,R}} = \mathbf{Q}_i \pm \frac{1}{2} \text{mm}(\mathbf{Q}_i - \mathbf{Q}_{i-1}, \mathbf{Q}_{i+1} - \mathbf{Q}_i) \quad (\text{A.3})$$

to be the values of \mathbf{Q} at the i th cell's left and right interface, respectively. In the above equations, the slope in each cell is determined by the nonlinear 'minmod' limiter defined as

$$\text{mm}(a, b) = \frac{1}{2} [\text{sgn}(a) + \text{sgn}(b)] \cdot \min(|a|, |b|), \quad (\text{A.4})$$

where $\text{sgn}(a) = |a|/a$ for any real $a \neq 0$, and it vanishes otherwise. The nonlinear limiter ensures that no spurious oscillations are introduced in the solution.

Upon extrapolating the cell interface values of \mathbf{Q} , we perform a non-conservative predictor time half-step to obtain the evolved cell interface values:

$$\bar{\mathbf{Q}}_i^{\text{L,R}} = \mathbf{Q}_i^{\text{L,R}} + \frac{1}{2} \frac{\Delta t^n}{\Delta x} [\mathbf{F}(\mathbf{Q}_i^{\text{L}}) - \mathbf{F}(\mathbf{Q}_i^{\text{R}})]. \quad (\text{A.5})$$

Then, we set up a local Riemann problem (RP), that is, a Cauchy problem with discontinuous initial data, on each cell interface of the grid. We continue by computing the flux through the cell interfaces from the solution to the local RPs.

In order to decrease the computational time and the complexity of the algorithm, we solve the RP at each interface by the approximate method of Harten, Lax and van Leer (HLL) (12, 13, 43). So, we take

$$\mathbf{F}_{i+\frac{1}{2}} \approx \mathbf{F}_{i+\frac{1}{2}}^{\text{HLL}} = \frac{S_{\text{R}}^+ \mathbf{F}(\bar{\mathbf{Q}}_i^{\text{R}}) - S_{\text{L}}^- \mathbf{F}(\bar{\mathbf{Q}}_{i+1}^{\text{L}}) + S_{\text{R}}^+ S_{\text{L}}^- (\bar{\mathbf{Q}}_{i+1}^{\text{L}} - \bar{\mathbf{Q}}_i^{\text{R}})}{S_{\text{R}}^+ - S_{\text{L}}^-}, \quad (\text{A.6})$$

where S_{L} and S_{R} (by assumption, $S_{\text{L}} \leq S_{\text{R}}$) denote (estimates of) the speed of the fastest- and slowest-moving waves in the solution of the RP, respectively, with $S_{\text{L}}^- = \min(0, S_{\text{L}})$ and $S_{\text{R}}^+ = \max(0, S_{\text{R}})$. Various choices for the wave speeds can be found in the literature (12, 13). Note that computing the intercell flux via (A.6) from the evolved data (A.5) used as the initial condition for RP constitutes a corrector time half-step, resulting in a scheme that is second-order accurate in time.

The stability of any explicit finite-difference method, such as the one described above, is contingent upon the Courant–Friedrichs–Lewy (CFL) condition, that is, the time step must be such that

$$S_{\text{max}}^n \Delta t^n \leq \Delta x \iff \Delta t^n = C_{\text{CFL}} \Delta x / S_{\text{max}}^n, \quad (\text{A.7})$$

where S_{max}^n denotes the speed of the fastest intercell wave at time $t = t^n$ and C_{CFL} the Courant–Friedrichs–Lewy number ($0 < C_{\text{CFL}} \leq 1$). In practice, the C_{CFL} is determined empirically so that the scheme is stable. According to this condition, a new time-step size Δt^n is determined at the end of each time step.

Furthermore, the physical problems that we solve in section 6 require the use of both transmissive and reflective BCs. These BCs are implemented via two ‘ghost’ cells (10, 12, 13) at each end of the grid.

Finally, all results in this paper are for $l = 3.0$ and $N = 4000$. Moreover, we chose $C_{\text{CFL}} = 1.0$ for the Euler equations, the IKE and the WNE; however, for the LWE we were forced to use $C_{\text{CFL}} = 0.3$ due to stability issues.

APPENDIX B

The evolution of an initial discontinuity in the acceleration for times before the formation of a shock is successfully described by the theory of singular surfaces (19, 25, 44). Since we carried out a detailed study of acceleration waves based on the (fully nonlinear) 1D Euler equations in (10, 11), we present here just a brief outline of these results for the convenience of the reader.

Consider a smooth planar surface $x = \Sigma(t)$ that is propagating, say, to the right, with speed (as measured by an observer at rest) $V(>0)$ along the x -axis of a Cartesian coordinate system. Let the speed of Σ with respect to the fluid, which we take to be a perfect gas, immediately ahead of it be $U(>0)$. Here, a ‘+’ superscript denotes the region into which Σ is advancing and a ‘−’ superscript denotes the region behind Σ . Furthermore, suppose that both u and ϱ are continuous functions of x and t , but that at least one of their first derivatives, say u_t , suffers a jump across Σ , that is, $[[u]] = [[\varrho]] = 0$, but $[[u_t]] \neq 0$. Here, $[[F]] \equiv F^- - F^+$, where for any function F we assume that $F^\mp \equiv \lim_{x \rightarrow \Sigma(t)^\mp} F(x, t)$ exist, and we note that F^\pm are at most functions of t only. If $F^- \neq F^+$, then Σ is termed a singular surface; and since $F = u_t$, the surface Σ is classified as an acceleration wave (19, 44). Given the above, and the value of $[[u_t]]$ at $t = 0$, we can determine $[[u_t]]$ for all later times using singular surface theory.

Using Hadamard’s lemma (19, 25, 45), and the assumptions $[[u]] = [[\varrho]] = 0$, we obtain

$$V[[u_x]] + [[u_t]] = 0, \quad V[[\varrho_x]] + [[\varrho_t]] = 0. \tag{B.1}$$

By taking jumps of the (dimensional) 1D Euler equations

$$\varrho_t + u\varrho_x + \varrho u_x = 0, \quad \varrho(u_t + uu_x) + \wp_x = 0, \tag{B.2}$$

employing the formula for the jump of a product, $[[\mathcal{A}\mathcal{B}]] = \mathcal{A}^+[[\mathcal{B}]] + \mathcal{B}^+[[\mathcal{A}]] + [[\mathcal{A}]][[\mathcal{B}]]$, and simplifying, we get the two additional jump relations

$$[[\varrho_t]] + u^+[[\varrho_x]] + \varrho^+[[u_x]] = 0, \quad \varrho^+[[u_t]] + \varrho^+u^+[[u_x]] + \wp_\varrho^+[[\varrho_x]] = 0. \tag{B.3}$$

Using (B.1) and (B.3)₁, we can express the jumps in ϱ_x , ϱ_t and u_x in terms of the jump in u_t . This yields, after simplifying and setting $A(t) \equiv [[u_t]]$,

$$[[u_x]] = -V^{-1}A, \quad [[\varrho_t]] = \frac{\varrho^+}{V - u^+}A, \quad [[\varrho_x]] = \frac{-\varrho^+}{V(V - u^+)}A. \tag{B.4}$$

Next, we recall the well-known expression for the wave speed:

$$V = u^+ \pm \sqrt{\wp_\varrho^+}, \tag{B.5}$$

where the ‘±’ cases refer to as ‘downstream’ and ‘upstream’ waves, respectively.

For definiteness, let us now assume that the gas ahead of Σ is in its equilibrium state. Thus, $u^+ = 0$, $\varrho^+ = \varrho_0$, $\wp_\varrho^+ = c_0^2$ and $\wp_{\varrho\varrho}^+ = c_0^2(\gamma - 1)/\varrho_0$, and $V = c_0$, where $c_0 \equiv \sqrt{\gamma \wp_0/\varrho_0}$ denotes the sound speed in the undisturbed gas. Omitting the details, it can be shown that the jump amplitude is governed by the following (quadratic) Bernoulli equation (10):

$$\frac{\mathcal{D}A}{\mathcal{D}t} - \Lambda_0 A^2 = 0, \tag{B.6}$$

the solution of which is

$$A(t) = \frac{A(0)}{1 - \Lambda_0 A(0)t}, \tag{B.7}$$

where $\Lambda_0 = c_0^{-1}(\gamma + 1)/2$ is a positive constant, the 1D displacement derivative $\mathcal{D}/\mathcal{D}t$ gives the time rate of change measured by an observer traveling with Σ and the value of $[[u_t]]$ at time $t = 0$ is denoted by $A(0) (\neq 0)$.

According to (B.7), the evolution of $A(t)$ can be qualitatively described as follows:

- (i) If $A(0) < 0$ [\Rightarrow that Σ is expansive (19)], then $A(t) \rightarrow 0$ from below as $t \rightarrow \infty$.
- (ii) If $A(0) > 0$ [\Rightarrow that Σ is compressive (19)], then $\lim_{t \rightarrow t_\infty} A(t) = \infty$, where the breakdown time t_∞ is given by $t_\infty = [\Lambda_0 A(0)]^{-1}$.

Note that case (ii) gives the condition for finite-time blow-up. Finally, in terms of the non-dimensional variables given in (2.4), the breakdown (or blow-up) time is given by $t_\infty = 2[\epsilon(\gamma + 1)A(0)]^{-1}$.